ESC European Society of Cardiology

Cardiovascular Research (2025) **121**, 760–774
https://doi.org/10.1093/cvr/cvaf039

Targeted delivery of TAPI-1 via biomimetic nanoparticles ameliorates post-infarct left ventricle function and remodelling

Qing Chen[1†], Yang Yu[1†], Lei Tong[1], Robert M. Weiss[1,2,3], and Shun-Guang Wei[1,2,3,4*]

[1]Department of Internal Medicine, University of Iowa Carver College of Medicine, 200 Hawkins Drive, Iowa City, IA 52242, USA; [2]Abboud Cardiovascular Research Center, University of Iowa Carver College of Medicine, 501 Newton Road, Iowa City, IA 52242, USA; [3]Veteran Affairs Medical Center, Research and Development, 601 HWY 6 WEST, Iowa City, IA 52246, USA; and [4]Iowa Neuroscience Institute, University of Iowa, 169 Newton Road, Iowa City, IA 52242, USA

Received 11 July 2024; revised 21 October 2024; accepted 22 January 2025; online publish-ahead-of-print 5 March 2025

Time of primary review: 65 days

See the editorial comment for this article 'Mimicked immunity: a strategy for targeted nanodrug delivery', by Y. Zhang *et al.*, https://doi.org/10.1093/cvr/cvaf050.

Aims The potential of nanoparticles as effective drug delivery tools for treating failing hearts in heart failure remains a challenge. Leveraging the rapid infiltration of neutrophils into infarcted hearts after myocardial infarction (MI), we developed a nanoparticle platform engineered with neutrophil membrane proteins for the targeted delivery of TAPI-1, a TACE/ADAM17 inhibitor, to the inflamed myocardium, aiming to treat cardiac dysfunction and remodelling in rats with MI.

Methods and results Neutrophil-mimic liposomal nanoparticles (Neu-LNPs) were constructed by integrating synthesized liposomal nanoparticles with LPS-stimulated neutrophil membrane fragments and then loaded with TAPI-1. MI rats were treated with TAPI-1 delivered via Neu-LNPs for 4 weeks. Left ventricular function was assessed by echocardiography and cardiac fibrosis was evaluated post-treatment. The novel Neu-LNPs maintained typical nanoparticle features, but with increased biocompatibility. Neu-LNPs demonstrated improved targeting ability and cellular internalization, facilitated by LFA1/Mac1/ICAM-1 interaction. Neu-LNPs displayed higher accumulation and cellular uptake by macrophages and cardiomyocytes in infarcted hearts post-MI, with a sustained duration. Treatments with TAPI-1-Neu-LNPs demonstrated greater protection against myocardial injury and cardiac dysfunction in MI rats compared to untargeted TAPI-1, along with reduced cardiac collagen deposition and expression of fibrosis biomarkers as well as altered immune cell compositions within the hearts.

Conclusions Targeted treatment with TACE/ADAM17 inhibitor delivered via biomimetic nanoparticles exhibited pronounced advantages in improving left ventricle function, mitigating cardiac remodelling, and reducing inflammatory responses within the infarcted hearts. This study underscores the effectiveness of Neu-LNPs as a drug delivery strategy to enhance therapeutic efficacy in clinical settings.

* Corresponding author. Tel: 319 384 4797; fax: 319 335 6969, E-mail: shunguang-wei@uiowa.edu

† The first two authors contributed equally to the study.

Graphical Abstract

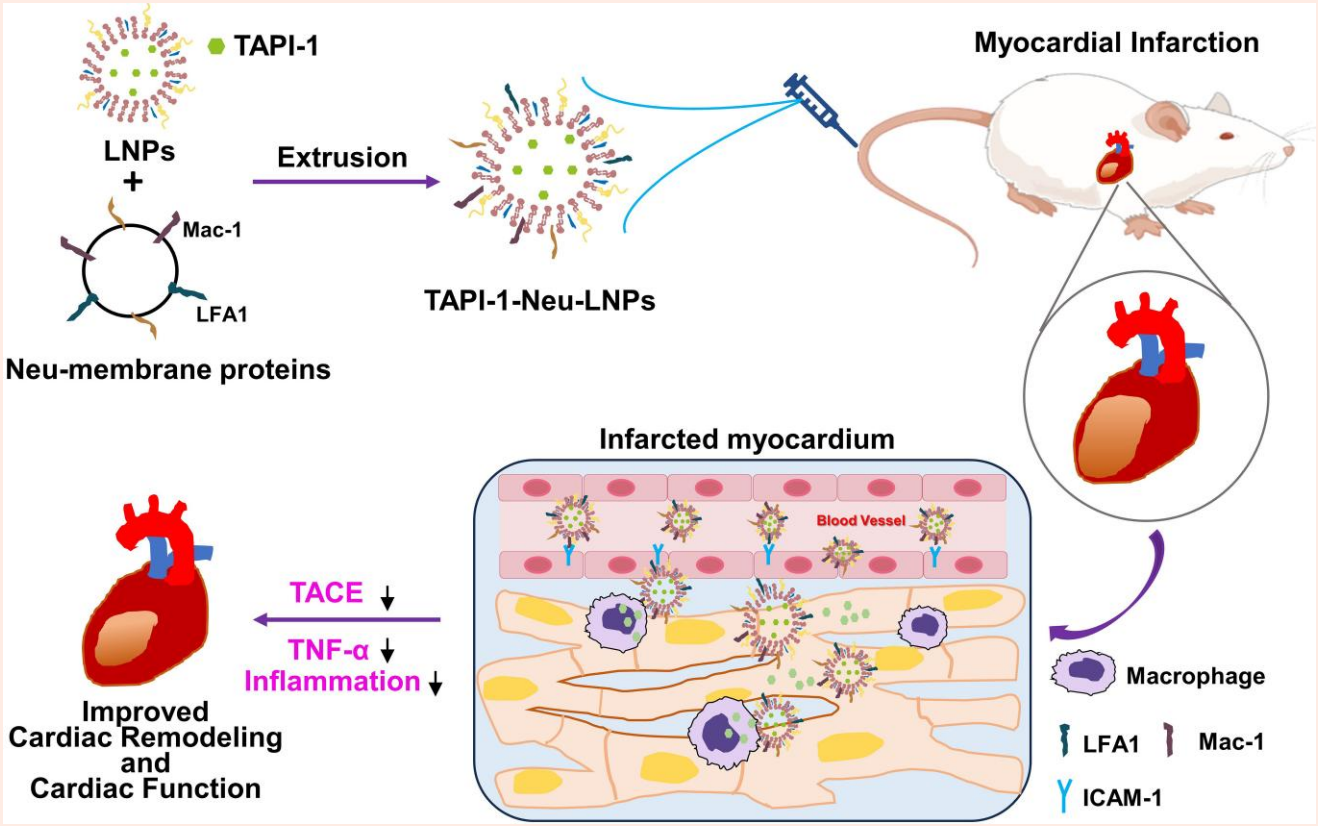

Keywords Myocardial infarction • Inflammation • TACE/ADAM17 • Nanotechnology • Drug delivery

1. Introduction

Nanotechnology has emerged as a revolutionary approach with immense potential to enhance the efficacy and effectiveness of therapeutic interventions in the medical field.[1,2] Due to their nanoscale size, high surface area-to-volume ratio, and unique physicochemical properties, nanoparticles can traverse biological membranes or blood–brain barriers to facilitate drug delivery, offering significant advantages in targeted treatment.[3] Furthermore, by optimizing parameters like pH and enzyme activity or surface modification with various functional moieties, nanoparticles can achieve controllable and targeted biodistribution properties to specifically address affected tissues or organs.[4,5] Currently, extensive research and development is underway for various types of nanoparticles catering to different medical applications.[6]

To address the concerns about cytotoxicity and limited biocompatibility associated with certain polymer materials, ongoing efforts are focused on developing cell-mimetic nanoparticles that utilize natural cell membranes.[7,8] These cell membrane-based nanoparticles offer enhanced bio-interfacing capabilities. By incorporating phospholipid bilayer membranes, the cell membrane proteins can be readily transported to the nanoparticle surface while preserving their functionality.[9,10] Additionally, this manipulation results in synthesized biomimetic nanoparticles exhibiting distinctive biological activities and retaining specific targeting properties from the source cells. Biomimetic drug carriers, particularly cell membrane-coated nanoparticles, have emerged as a promising therapeutic platform for the treatment of cardiovascular diseases.[11,12]

Among the main types of nanoparticles, liposomes have demonstrated passive targeting abilities to inflammatory sites through the enhancing permeability and retention (EPR) effect.[13] Their circulation time can be prolonged, especially when PEGylation (polyethylene glycol) is applied to hinder phagocytosis by monocyte-macrophages in the blood.[14] In the context of heart failure (HF)-induced by myocardial infarction (MI), characterized by immune activation and heightened inflammation, immune cells infiltrate the injured cardiac myocytes to orchestrate inflammatory responses. Notably, neutrophils (Neu) are among the first immune cells to infiltrate the damaged area,[15] making their inflammatory chemotactic capability a promising approach for enhancing drug targeting potentials.

In the present study, using these design strategies, we developed a novel formulation of PEG_{2000}-liposomal nanoparticles (LNPs) coated with neutrophil membrane fragments as a drug delivery tool for a pharmaceutical agent TAPI-1, specifically targeting the injured heart in rats with MI. TAPI-1 is a potent inhibitor of tumour necrosis factor-α (TNF-α) converting enzyme (TACE/ADAM17), which is involved in the production of inflammatory soluble TNF-α.[16] Previous studies have demonstrated that central inhibition of TACE activity exhibits a beneficial role in reducing neuroinflammation and ameliorating sympathetic activation in HF rats.[17,18] The main objectives of this work were: (i) to evaluate the enhanced targeting potential of neutrophil-mimic liposomal nanoparticles (Neu-LNPs) as a drug delivery vehicle specifically targeting inflamed tissues of the injured heart in rats with MI; and (ii) to examine the efficacy and effectiveness of Neu-LNPs loaded with TAPI-1 (TAPI-1-Neu-LNPs) administered intravenously as a therapeutic approach for improving cardiac dysfunction and remodelling in the treatment of MI-induced HF. Overall, this work provides a comprehensive assessment of biomimetic nanoparticles for targeted drug delivery in treating MI rats.

2. Methods

A detailed description of the methods is provided in the Supplementary material online, *Methods*.

2.1 Animals

The experimental protocols in this study were approved by the University of Iowa Institutional Animal Care and Use Committee and conducted in accordance with the National Institutes of Health '*Guide for the Care and Use of Laboratory Animals*.' Experiments were carried out on male adult Sprague-Dawley rats (300–350) purchased from Envigo/Harlan Sprague Dawley (Indianapolis, IN). The animals had *ad libitum* access to standard rat chow and tap water. These rats were housed in a temperature- (23 ± 2°C) and light-controlled (12:12 h light-dark cycle) animal care facility on the University of Iowa Health Science Campus. All possible measures were taken to minimize both the number of animals used and any potential suffering they might experience.

2.1.1 Induction of MI

Rats were anaesthetized (ketamine 90 mg/kg and xylazine 10 mg/kg ip) and underwent surgery under aseptic conditions to ligate the left coronary artery to induce MI, or an identical surgical procedure without ligating the left coronary artery to produce control (SHAM) rats, as previously described.[19,20]

2.2 Assessments of cardiac function and remodelling

2.2.1 Echocardiography

Rats were tranquilized with ketamine (60 mg/kg ip) and underwent two-dimensional echocardiography to assess left ventricular (LV) function. The ischaemic zone (IZ) as a percentage of LV circumference (% IZ), LV ejection fraction (LVEF), LV end-diastolic volume (LVEDV), and LV end-systolic volume (LVESV) were calculated from the echocardiographic data. Compared with SHAM rats, rats with HF had reduced LVEF and increased LVEDV and LVESV.

2.2.2 Cardiac haemodynamic and anatomical assessments

Under anaesthetized condition, a Millar Mikro-tip catheter (Millar, Houston, TX) was inserted into the right carotid artery and advanced retrogradely towards the aorta and then into the LV to measure peak systolic pressure (LVPSP), end-diastolic pressure (LVEDP), and the maximal rate of change in LV systolic pressure over time during isovolumetric contraction ($+dP/dt_{max}$) and relaxation ($-dP/dt_{max}$).

The heart and wet lung were then collected and weighed. Heart weight (HW)-to-body weight (BW) and wet lung weight (LW)-to-BW ratios were determined as indicators of cardiac remodelling and pulmonary congestion.

2.2.3 Histological analysis of cardiac fibrosis

Cardiac fibrosis in peri-infarct areas was analysed by slicing frozen heart tissue into 7 μm sections, staining with Masson's trichrome. Fibrosis was quantified using ImageJ software, with 12 images from six cross-sections per animal used for statistical analysis.

2.3 Experimental protocols

Echocardiography was performed within 24 h after coronary artery ligation to induce MI or sham operation procedure, and repeated at the conclusion of the 4-week protocol. MI rats with a small MI on the initial echocardiogram (ischaemic zone ≤30%) or died before the end of the protocol were excluded from the study. SHAM and MI rats with ischaemic zone > 30% were randomly assigned into treatment groups ($n = 6–7$ in each group) according to the following assignments. The estimated infarct zone and LVEF were well matched among the MI groups.

2.3.1 Assessments of LV function and cardiac remodelling

(i) SHAM + vehicle (VEH); (ii) MI + VEH; (iii) MI + TAPI-1; (iv) MI + Neu-LNPs; (v) MI + TAPI-1-LNPs; and (vi) MI + TAPI-1-Neu-LNPs. TAPI-1-loaded biomimetic nanoparticles (3.3 mg, containing 50 μg of TAPI-1), TAPI-1 (50 μg) or VEH were systemically administered via tail veins every other day for 4 weeks. At the end of the experiments, a second echocardiogram was performed to determine treatment effects. These rats were anaesthetized with urethane (1.5 g/kg ip) for assessments of cardiac haemodynamics and anatomical changes, and then euthanized by decapitation to harvest blood, heart, and lung for histological, molecular, and flow cytometric analyses. The levels of TNF-α and TACE activity were also assessed in some animals.

2.3.2 Targeting and cellular uptake analysis of Neu-LNPs

To investigate the targeting mechanisms of Neu-LNPs mediated by neutrophil membrane proteins, specifically lymphocyte function-associated antigen 1 (LFA-1, CD11a/CD18) and macrophage-1 antigen (Mac-1, CD11b/CD18), Dil-labelled Neu-LNPs were injected into rats via tail veins in the following experimental groups: (i) SHAM + Dil-labelled Neu-LNPs; (ii) MI + Dil-labelled Neu-LNPs; and (iii) MI + Dil-labelled Neu-LNPs + CD18 antibody. Twenty-four hours after injection, the rats were perfused with PBS under anaesthesia, and then euthanized by decapitation to collect the heart for fluorescence analysis and immunofluorescent staining.

2.4 Preparation of Neu-LNPs

2.4.1 Synthesis of Neu-LNPs

To synthesize liposomal nanoparticles, a mixture of 1-palmitoyl-2-oleoyl-sn-glycero-3-phosphocholine (POPC), 1-palmitoyl-2-oleoyl-sn-glycero-3-phosphoethanolamine (POPE)-PEG_{2000}, and cholesterol was dissolved in 100 μL reagent-grade chloroform along with 30 μL of reagent-grade methanol, at a ratio of 7:1.5:1.5 (mol/mol/mol). The organic solvent was evaporated under a nitrogen flow, leaving behind a thin lipid film in the glass vial. The thin lipid film was then hydrated with PBS in a water bath at 55°C for 30 min. Subsequently, the nanoparticles were sonicated for 10 min and then subjected to probe sonication for an additional 3 min to create liposomes and ensure proper size and homogeneity. Neu-LNPs were constructed by adding LPS-stimulated neutrophil membrane fragments to the synthesized liposomal nanoparticles. The mixture was subjected to ultrasonication for 10 min to facilitate the fusion of neutrophil membrane fragments into the lipid membranes.[21] The coated-liposomes were then centrifuged at 3000 *g* for 15 min to remove any redundant materials and obtain purified Neu-LNPs for further use.

2.4.2 Drug loading

To load TAPI-1 into Neu-LNPs, TAPI-1 was first dissolved in DMSO and then diluted with chloroform to a concentration of 1 mg/mL. This TAPI-1 solution was then added to the chloroform solution of lipids before the evaporation process using a nitrogen flow. The subsequent steps for Neu-LNPs preparation remained the same as described above. For drug loading analysis, a TAPI-1 standard solution was prepared with PBS, and its wavelength was measured using a fluorescence spectrophotometer (Molecular Devices, USA) to draw a standard curve. The TAPI-1-loaded nanoparticles were demulsified with methanol (at a ratio of 1 mL:1 mL) and measured using the same fluorescence spectrophotometer. The TAPI-1 loading efficiency was then calculated using the standard curve. The Drug Loading (DL) was calculated using the following formula: DL(%) = Drug/(Drug + Lipid Materials) × 100%.

2.5 Characterization of Neu-LNPs

2.5.1 Physical characteristics

To characterize the Neu-LNPs, hydrodynamic diameters, zeta potential, and polydispersity index (PDI) were measured using dynamic light

scattering technology with a Malvern Zetasizer instrument (Nano ZS, Malvern). The morphologies of the nanoparticles were observed using transmission electron microscopy (TEM).

2.5.2 Isolation and verification of neutrophil membrane-associated proteins on Neu-LNPs

Fresh rat neutrophils were isolated from bone marrow and purified using density gradient centrifugation. After red blood cell lysis and PBS washing, the neutrophils were centrifuged in a gradient buffer and stimulated with lipopolysaccharide (LPS). Post-stimulation, cells were lysed, and the supernatant underwent multiple centrifugation steps to remove cellular debris, mitochondria, and nuclei. The final pellets were stored for subsequent use, with protein concentration measured by BCA assay. Verification of neutrophil membrane proteins on Neu-LNPs involved freeze-drying nanoparticles, FTIR spectroscopy, and western blotting to detect CXCR4 and CD11a, ensuring the presence of specific neutrophil proteins.

2.5.3 Cellular uptake and binding analysis of Neu-LNPs

H9C2 cells and HUVECs were incubated with LPS and varying ratios of Dil-loaded Neu-LNPs. After incubation, the cells were washed, trypsin-digested, and subjected to flow cytometry to analyse cellular uptake. For binding analysis, LPS-treated cells were incubated with anti-CD18 antibody and Dil-labelled Neu-LNPs. Post-incubation, cells were washed, fixed, and stained for ICAM-1. Confocal microscopy was used to observe the results, confirming cellular binding and uptake of Neu-LNPs in H9C2 and HUVEC cells.

2.5.4 *In vivo* imaging of Neu-LNPs biodistribution

Dir-labelled Neu-LNPs or LNPs were administered to observe biodistribution via photoacoustic imaging at various time points. *Ex vivo* imaging of major organs was conducted to assess distribution, analysed using the Xenogen IVIS 200 system, highlighting targeted delivery and uptake of Neu-LNPs.

2.5.5 *In vivo* targeting and cellular uptake analysis of Neu-LNPs

Dil-labelled Neu-LNPs were injected into MI and SHAM rats via the tail vein. To block neutrophil membrane proteins LFA-1 and Mac-1, anti-CD18 antibody was incubated with Dil-labelled Neu-LNPs before injection into MI rats. Twenty-four hours post-injection, hearts were collected, embedded in OCT, sectioned into 7 μm slices, and stained with DAPI. Dil-labelled Neu-LNPs in the peri-infarct zone of the left ventricular myocardium were visualized using confocal microscopy. To assess Neu-LNP uptake by macrophages and cardiomyocytes, heart sections from MI rats were stained with F4/80 (macrophages) and cardiac troponin T (cardiomyocytes). Immunofluorescent images were visualized using confocal microscopy.

2.6. Statistical analysis

Data were presented as mean ± S.E.M. Analyses of the data were conducted by investigators who were blinded to the experimental conditions. Kolmogorov–Smirnov test and Levene's test were performed to verify normal distributions and equal variances, respectively. Unpaired Student's *t*-test, one-way or two-way Analysis of Variance (ANOVA) followed by multiple comparison tests were applied to determine statistical significance. $P < 0.05$ was considered statistically significant.

3. Results

3.1 Preparation of Neu-LNPs

The procedure of Neu-LNPs preparation is depicted in *Figure 1A*. Liposomal nanoparticles were synthesized using a combination of POPC, cholesterol, and POPE-PEG_{2000}. TAPI-1 was loaded into the PEG_{2000}-liposomes using the thin film hydration method.[22] Bone marrow-derived neutrophil cells were purified using Ficoll-paque plus gradient cell separation solution.[23] Flow cytometric analysis revealed that the purity of the isolated neutrophils exceeded 80% (see Supplementary material online, *Figure S1*). The isolated neutrophils were further confirmed by demonstrating their positivity for the neutrophil marker CD11b, while being negative for CD11c (a marker of dendritic cells) and F4/80 (a marker of murine macrophages). Neu-LNPs were created by integrating the synthesized liposomes with membrane fragments of LPS-stimulated neutrophils. The capacity of Neu-LNPs to elicit inflammatory responses was examined in cultured H9C2 cells. Our findings indicated that while LPS significantly increased the levels of cytokines TNF-α and interleukin-6, the synthesized Neu-LNPs did not induce the production of these inflammatory molecules, suggesting that Neu-LNPs had a minimal effect in causing inflammation (see Supplementary material online, *Figure S2*).

3.2 Characterization of Neu-LNPs

Considering multiple factors, including their size (*Figure 1B*), zeta potential (*Figure 1C*), polydispersity index (PDI, *Figure 1D*), and their potential for cellular internalization, a ratio of 0.5:1 of neutrophil fragments to liposomal nanoparticles was selected and employed for subsequent study. Neu-LNPs created at this ratio exhibited an increase in diameter (130 ± 1.73 nm vs. 88 ± 1.77 nm) and a reduction in zeta potential (−5.4 ± 0.5 mV vs. −1.9 ± 0.2 mV) when compared with LNPs, implying the successful integration of neutrophil membrane proteins onto the liposomes, while still maintaining the characteristics of a standard nanoparticle. The typical images of LNP and Neu-LNP by TEM showed a spherical morphology with the sizes at ∼90 and ∼110 nm, respectively (*Figure 1E*). Although the size of Neu-LNPs appeared larger following fusion with neutrophil fragments than LNPs, neither Neu-LNPs nor LNPs exhibited significant size changes over a 14-day period (*Figure 1F*), suggesting their inherent stability.

To validate the successful integration of neutrophil membrane proteins onto the liposomal nanoparticles, the vibrational characteristics and chemical signatures of the protein profile within Neu-LNPs were assessed through FTIR spectroscopy. As illustrated in *Figure 1G*, while both the amide I band, indicative of C=O stretching vibrations (within the range of 1700–1600 cm^{-1}) and the amide II band, relevant to N–H bending and C–N stretching vibrations (within the range of 1580–1510 cm^{-1})[24] were present in all three samples, the distinctive absorption bands associated with glycosylated neutrophil membrane proteins (within the range of 1200–900 cm^{-1})[25] were exclusively detected in Neu-LNPs but not in LNPs.

3.3 Cytotoxicity of Neu-LNPs

In vitro cytotoxicity assessment of Neu-LNPs was conducted using the CCK-8 assay. The viability of cells, serving as an indicator of cytotoxicity and biocompatibility, was evaluated in HUVECs and H9C2 (*Figure 1H*) cells following incubation with varying concentrations of Neu-LNPs, ranging from 1 ng/mL to 0.2 mg/mL. We found that cell viability remained consistently above 80% at both 24 and 48 h following the introduction of Neu-LNPs. This robust cell viability underscores the pronounced biocompatibility and minimal cytotoxicity of Neu-LNPs. In terms of drug loading, both Neu-LNPs and LNPs exhibited comparable capability to encapsulate TAPI-1, with loading amounts of 0.058 ± 0.002 mg and 0.052 ± 0.004 mg, respectively. The drug loading percentages (DL%) were measured at 1.5 ± 0.06% for Neu-LNPs and 1.89 ± 0.14% for LNPs, demonstrating their potential as carriers for therapeutic agents.

3.4 Cellular uptake analysis of Neu-LNPs

To assess the potential for cellular uptake of Neu-LNPs, HUVECs and H9C2 cells were exposed to Neu-LNPs containing varying proportions of Neu-membrane fragments. Compared with LNPs without Neu-fragments, all Neu-LNPs containing membrane proteins exhibited a notable increase in cellular uptake of proteins. Confocal images indicated that higher protein ratios generally correlated with enhanced endocytic activity (see Supplementary material online, *Figure S3*). Remarkably, at a protein-to-LNPs ratio of 0.5:1, the internalization process reached a saturation point in both HUVECs (*Figure 2A*) and H9C2 cells (*Figure 2D*), with negligible changes compared to the

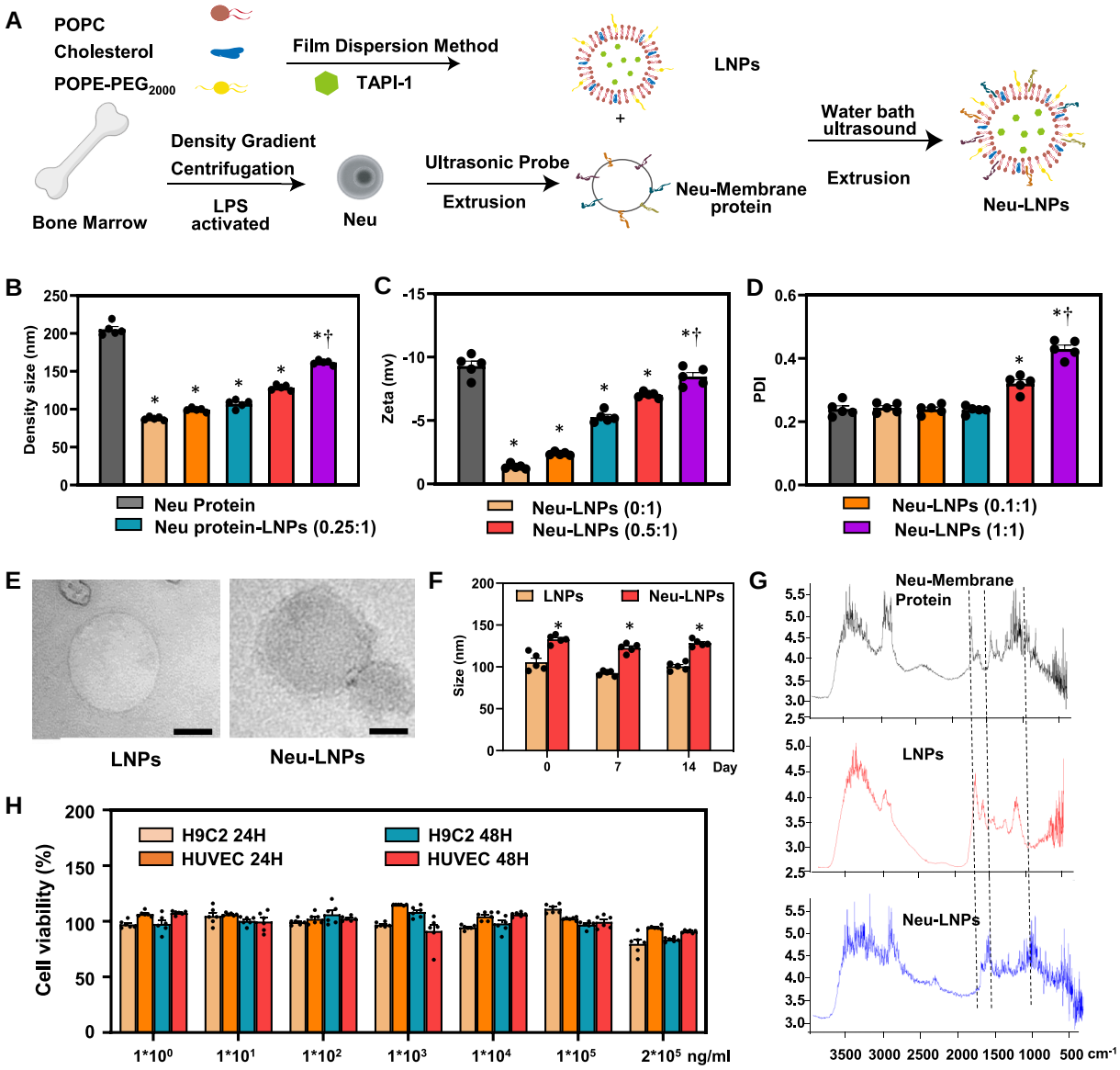

Figure 1 Fabrication and characterization of Neu-LNPs. (*A*) Schematic outlining the procedure of Neu-LNPs preparation. The characteristics of Neu-LNPs with varying ratios of neutrophil membrane proteins to LNPs were assessed by size (*B*), zeta potential (*C*), and PDI (polymer dispersity index, *D*). *$P < 0.05$ vs. Neu-Protein, †$P < 0.05$ vs. Neu-LNPs (0.5:1). (*E*) Transmission electron microscopy (TEM) images of typical LNPs and Neu-LNPs. Scale bars: 50 nm. (*F*) Grouped data showing TEM analysis of the density size of LNPs and Neu-LNPs at 0, 7, and 14 days indicate size stabilization within a two-week duration despite a difference in diameter between LNPs and Neu-LNPs (*$P < 0.05$). (*G*) Fourier-transform infrared (FTIR) spectroscopy analysis of neutrophil membrane, LNPs and Neu-LNPs. (*H*) Cytotoxicity of Neu-LNPs assessed by cell viability in HUVECs and H9C2 cells. Data set was analysed with one-way ANOVA followed by Tukey's multiple comparisons for *B–D* and *H* and with unpaired Student's *t*-test for *F*. $n = 5–6$ in each group.

protein-to-LNPs ratio at 1:1. This finding was substantiated by flow cytometry analysis, which indicated a greater cellular uptake in both HUVECs (*Figure 2B* and *C*) and H9C2 cells (*Figure 2E* and *F*) at the ratio of 0.5:1, as evidenced by an increase in fluorescence intensity.

3.5 Targeting and binding analysis of Neu-LNPs *in vitro*

The Transwell model was utilized to assess the permeability of Neu-LNPs through endothelial layers towards cardiomyocytes (*Figure 3A*). The uptake of Dil-labelled Neu-LNPs or LNPs within the H9C2 cells was visualized through fluorescence images (see Supplementary material online, *Figure S4*). When compared to non-stimulated HUVECs, the cellular uptake of either Neu-LNPs or LNPs displayed no significant disparity in LPS-stimulated cells. However, within LPS-stimulated HUVECs, the internalization of Neu-LNPs was notably augmented in comparison to LNPs (*Figure 3B*). The heightened uptake of Neu-LNPs was similarly observed in H9C2 cells, surpassing the uptake of Neu-LNPs in non-stimulated cells and that of LNPs in both stimulated and non-stimulated cells (*Figure 3C*). Neu-LNPs typically enter these cells via endocytosis and are primarily transported to endosomes, where they ultimately fuse with lysosomes. These findings suggest that, particularly under inflammatory states, the

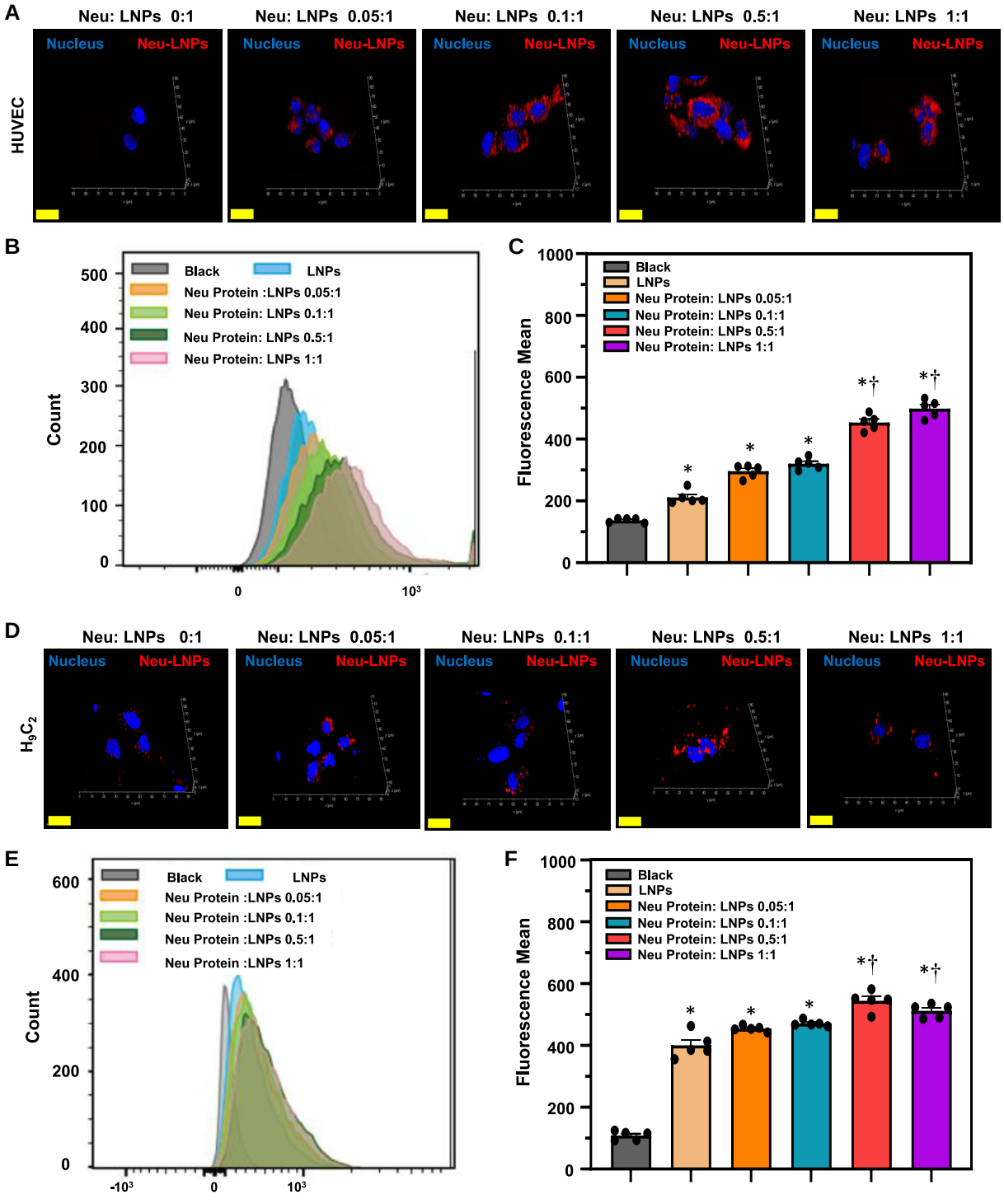

Figure 2 Assessment of cellular uptake for Neu-LNPs. (*A*) Three-dimensional confocal images illustrating the cellular internalization of Neu-LNPs with varying ratios of neutrophil membrane proteins to LNPs in HUVECs. Flow cytometric evaluation of cellular uptake of Neu-LNPs in HUVECs, presented as flow cytometry images (*B*) and grouped data shown as fluorescence intensity (*C*). (*D*) Three-dimensional confocal images illustrating the cellular internalization of Neu-LNPs with varying ratios of neutrophil membrane proteins to LNPs in H9C2s. Flow cytometric evaluation of cellular uptake of Neu-LNPs in H9C2s, presented as flow cytometry images (*E*) and grouped data (*F*). Scale bars: 20 μm. $n = 5$ in each group, $^{*}P < 0.05$ vs. black, $^{\dagger}P < 0.05$ vs. Neu-Protein: LNPs 0.1:1. Data set was analysed with one-way ANOVA followed by Tukey's multiple comparisons for *C* and *F*.

incorporation of neutrophil proteins significantly enhances the transport of liposomes across the endothelial monolayer, promoting their passage through the endothelial barrier.

CXCR4 and CD11a represent two distinctive proteins associated with neutrophils that may possess chemotactic capabilities. Western blot analysis displayed the presence of both proteins in Neu-LNPs (*Figure 3D*) while

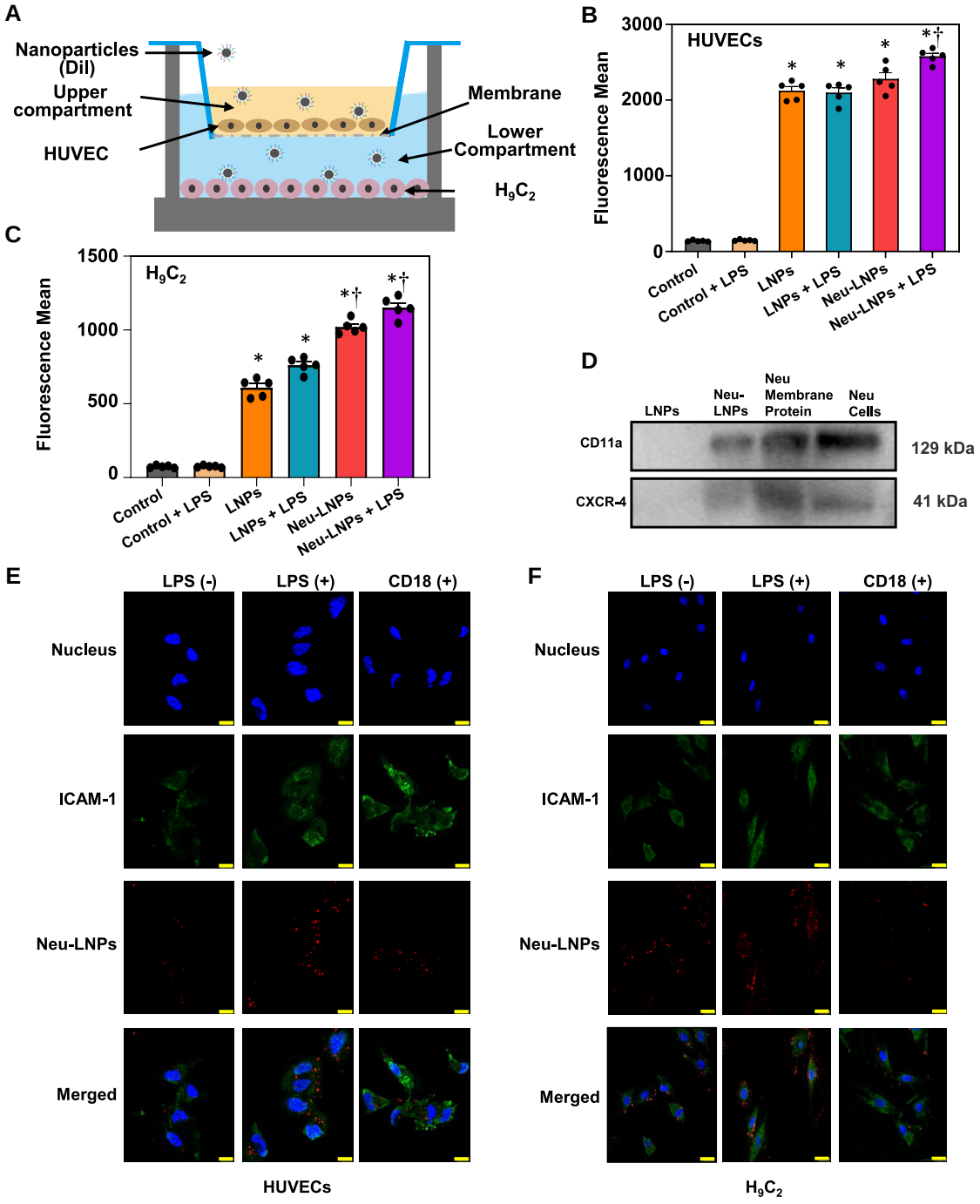

Figure 3 Targeting and binding analysis of Neu-LNPs *in vitro*. (*A*) Schematic representation of the endothelial-inflamed cardiomyocytes Transwell model utilized for targeting and binding analysis of Neu-LNPs. (*B*, *C*) Quantitative data depicting the cellular uptake of LNPs/Neu-LNPs by apical HUVECs or baso-lateral H9C2s using flow cytometric analysis, presented as fluorescence mean. (*D*) Western blot analysis confirming the presence of CXCR4 and CD11a in Neu-LNPs. (*E*, *F*) Confocal images showing the up-regulated expression of ICAM-1 and enhanced uptake of Neu-LNPs by LPS-stimulated HUVECs or H9C2s, with inhibition of LFA1/Mac-1 by anti-CD18 antibody leading to reduced uptake. ICAM-1, intercellular cell adhesion molecule-1; LFA1, lymphocyte function-associated antigen 1; Mac-1, macrophage-1 antigen. Scale bars: 10 μm. $n = 5$ in each group, $^{*}P < 0.05$ vs. control, $^{\dagger}P < 0.05$ vs. LNPs + LPS or LNPs. Data set was analysed with one-way ANOVA followed by Tukey's multiple comparisons for *B* and *C*.

they were absent in LNPs, confirming the successful fusion of neutrophil membrane proteins with liposomes. In another *in vitro* approach, cultured HUVECs or H9C2 cells were stimulated with LPS to induce inflammatory responses, simulating an inflamed environment. Following LPS treatment, the expression of intercellular adhesion molecule-1 (ICAM-1), the binding protein for LFA-1 and Mac-1, was significantly up-regulated in both HUVECs and H9C2 cells. Upon introducing DiI-labelled Neu-LNPs, a significantly heightened endocytosis in LPS-treated HUVECs (*Figure 3E*) or

H9C2 cells was observed (*Figure 3F*). Furthermore, when LFA1/CD11a and Mac1/CD11b on the Neu-LNPs were obstructed using an anti-CD18 antibody, the uptake of Neu-LNPs by HUVECs (*Figure 3E*) or H9C2 cells (*Figure 3F*) was significantly reduced.

3.6 Targeting and cellular uptake analysis of Neu-LNPs *in vivo*

To further elucidate the involvement of neutrophil receptor proteins LFA-1 and Mac-1 in enhancing the targeting efficacy of Neu-LNPs towards infarcted hearts, we conducted an *in vivo* study examining the effects of inhibiting LFA-1 and Mac-1 using anti-CD18 antibody on the distribution of Neu-LNPs within the myocardium of MI rats. We found that LV myocardium surrounding the infarct zone of MI rats treated with Dil-labelled Neu-LNPs exhibited a substantial accumulation of Neu-LNPs compared to SHAM rats. However, when LFA-1 and Mac-1 were blocked by anti-CD18 antibody, the presence of Neu-LNPs markedly diminished in MI rats (*Figure 4A*). In MI rats, the injected Neu-LNPs primarily accumulated in the border region of infarct zone in left ventricular, rather than in the right ventricle (see Supplementary material online, *Figure S5*). The cellular uptake of Neu-LNPs in MI hearts was examined through immunofluorescent staining. Confocal images revealed the presence of Dil-labelled Neu-LNPs in both macrophages (*Figure 4B*) and cardiomyocytes (*Figure 4C*) in the peri-infarct zone of MI rats, both of which are the major producing cells for TNF-α in the inflamed heart.[26,27] These observations collectively support the nation that the interaction between LFA1/Mac1 and ICAM-1 likely plays a crucial role in facilitating the transport of Neu-LNPs to inflammatory sites.

3.7 Biodistribution of Neu-LNPs *in vivo*

To evaluate the *in vivo* distribution of liposomal nanoparticles, Dir-labelled Neu-LNPs and LNPs were administered intravenously via the tail veins in rats, and their distribution was monitored over a 48 h period. As depicted in *Figure 5A* and *B*, Neu-LNPs were discernible in the heart of MI rats within 2 h after administration, reaching their peak concentration at 8 h post-injection. This presence persisted for at least 48 h and potentially even longer. The Dir-labelled Neu-LNPs and LNPs in the heart of MI rats could be detectable at 96 h after injection (see Supplementary material online, *Figure S6*). *Ex vivo* imaging of isolated hearts indicated that Neu-LNPs predominantly accumulate in the infarct zone and surrounding areas, rather than being distributed throughout the entire heart (see Supplementary material online, *Figure S7*). Compared with Dir alone, Dir-labelled Neu-LNPs displayed an extended circulation profile in the bloodstream in MI rats, reinforcing the potential of Neu-LNPs for therapeutic efficacy. Additionally, the fluorescence intensity of Dir-labelled Neu-LNPs in the hearts of MI rats was approximately 10–20 times higher than that in MI rats injected solely with Dir, across all the time points examined. In contrast, Neu-LNPs scarcely accumulated in the healthy hearts of SHAM rats. Furthermore, in comparison to MI rats treated with LNPs, MI rats injected with Neu-LNPs also exhibited stronger and more enduring fluorescence intensity within the heart. These observations underscore the enhanced targeting and long-lasting efficacy of Neu-LNPs in homing to the infarcted heart of MI rats.

Upon completion of the 48 h monitoring period, the hearts, livers, spleens, lungs, and kidneys were harvested for *ex vivo* tissue imaging. Notably, a significant accumulation of Neu-LNPs was observed in the hearts of MI rats. The fluorescence intensity of Neu-LNPs was approximately two-fold greater in comparison to LNPs, and three-fold higher compared to both vehicle (Dir)-treated MI rats or SHAM rats treated with Neu-LNPs (*Figure 5C* and *D*). An *ex vivo* biodistribution analysis of Neu-LNPs or LNPs in other organs including livers, spleens, lungs, and kidneys indicated that most of the nanoparticles were congregated in the liver (see Supplementary material online, *Figure S8*), given its primary function as a metabolic organ of the body.

3.8 Effect of TAPI-1-Neu-LNPs on cardiac function and haemodynamics

The timeline of experimental procedure and analysis was illustrated in *Figure 6A*. The dose of TAPI-1 loaded into the Neu-LNPs was derived from our previous studies[17,18] and those of others,[28] and optimized based on the loading capacity of Neu-LNPs. The efficiency of TAPI-1-Neu-LNPs in reducing TACE activity and TNF-α levels was evaluated in this study. Compared to SHAM rats, MI rats treated with the vehicle displayed significantly elevated levels of TACE activity in the border regions of the infarcted zones. However, the levels of TACE activity in MI rats treated with TAPI-1-Neu-LNPs were significantly reduced (*Figure 6B*). Additionally, treatment with TAPI-1-Neu-LNPs in MI rats resulted in attenuated levels of TNF-α in both infarcted heart tissues and blood compared to vehicle-treated MI rats (*Figure 6C*). Echocardiography performed within 24 h after MI, prior to any treatments, revealed that IZ, LVEF, LVESV, and LVEDV were similar in all five MI groups. At 4 weeks after MI, these variables were further compromised with decreased LVEF and ischaemic zone, and increased LVESV and LVEDV in MI rats treated with TAPI-1, TAPI-1-LNPs, Neu-LNPs, or VEH (*Figure 6D*). However, the 4-week treatment with TAPI-1-Neu-LNPs prevented the reduction of LVEF in the MI rats, and lessened the further increment of LVESV and LVEDV when compared with the measurements within 24 h after MI. Furthermore, ischaemic zone size quantified by echocardiography decreased over time in MI rats treated with TAPI-1-Neu-LNPs, but not the MI rats in other treatment groups. More importantly, at the conclusion of the study protocols, the aforementioned indexes for cardiac function were significantly improved in MI rats treated with TAPI-1-Neu-LNPs, compared with untargeted TAPI-1 or control groups (*Figure 6D*, Supplementary material online, *Table S1*).

Haemodynamic measurements revealed that heart rate (HR, *Figure 6E*) was comparable across all five HF treatment groups and SHAM rats. Systolic blood pressure (SBP, *Figure 6E*) and LVPSP were significantly decreased in MI rats treated with vehicle or TAPI-1 alone when compared with vehicle-treated SHAM rats. Treatments with Neu-LNPs, TAPI-1-LNPs, or TAPI-1-Neu-LNPs ameliorated but did not reverse the reduction in SBP and LVPSP in MI rats. LVEDP was elevated in all MI rats, compared to SHAM. Treatment with TAPI-1-Neu-LNPs, but not with untargeted TAPI-1, ameliorated the increase in LVEDP, compared to treatment with vehicle (*Figure 6E*). Additionally, cardiac contractility indicated by LV dP/dt_{max} was significantly lower in all MI groups compared to SHAM (*Figure 6E*). Although a 4-week treatment with TAPI-1, Neu-LNPs, or TAPI-1-LNPs tended to improve LV dP/dt_{max}, it did not obtain the statistical significance. However, MI rats treated with TAPI-1-Neu-LNPs significantly elevated LV dP/dt_{max} in systolic (+) or diastolic (−) phase compared with MI rats treated with VEH, suggesting an improvement in LV systolic and diastolic function.

3.9 Effect of TAPI-1-Neu-LNPs on anatomic indicators

The ratios of HW to BW and LW to BW were used to evaluate cardiac remodelling and pulmonary congestion, respectively. The typical images of the lung and heart taken from each treatment group at the end of the experiments were shown in *Figure 7A*. Although body weight was similar among the experimental groups, the ratios of HW to BW and LW to BW were substantially higher in VEH-treated MI rats compared with VEH-treated SHAM rats. After a 4-week treatment, both ratios were significantly reduced in TAPI-1-Neu-LNPs treated but not in TAPI-1, Neu-LNPs, or TAPI-1-LNPs treated MI rats (*Figure 7B* and *C*), indicating an improvement in cardiac remodelling and pulmonary oedema.

Histological analysis by Masson staining showed that the cross-sectional area of collagen deposition, an indicator of cardiac fibrosis, was robustly increased in the peri-infarcted area of LV in MI rats compared with SHAM rats. *MI* rats treated with TAPI-1-Neu-LNPs had significantly decreased collagen deposition in the peri-infarcted area of LV compared with MI rats treated with VEH, TAPI-1, Neu-LNPs, or TAPI-1-LNPs (*Figure 7D*

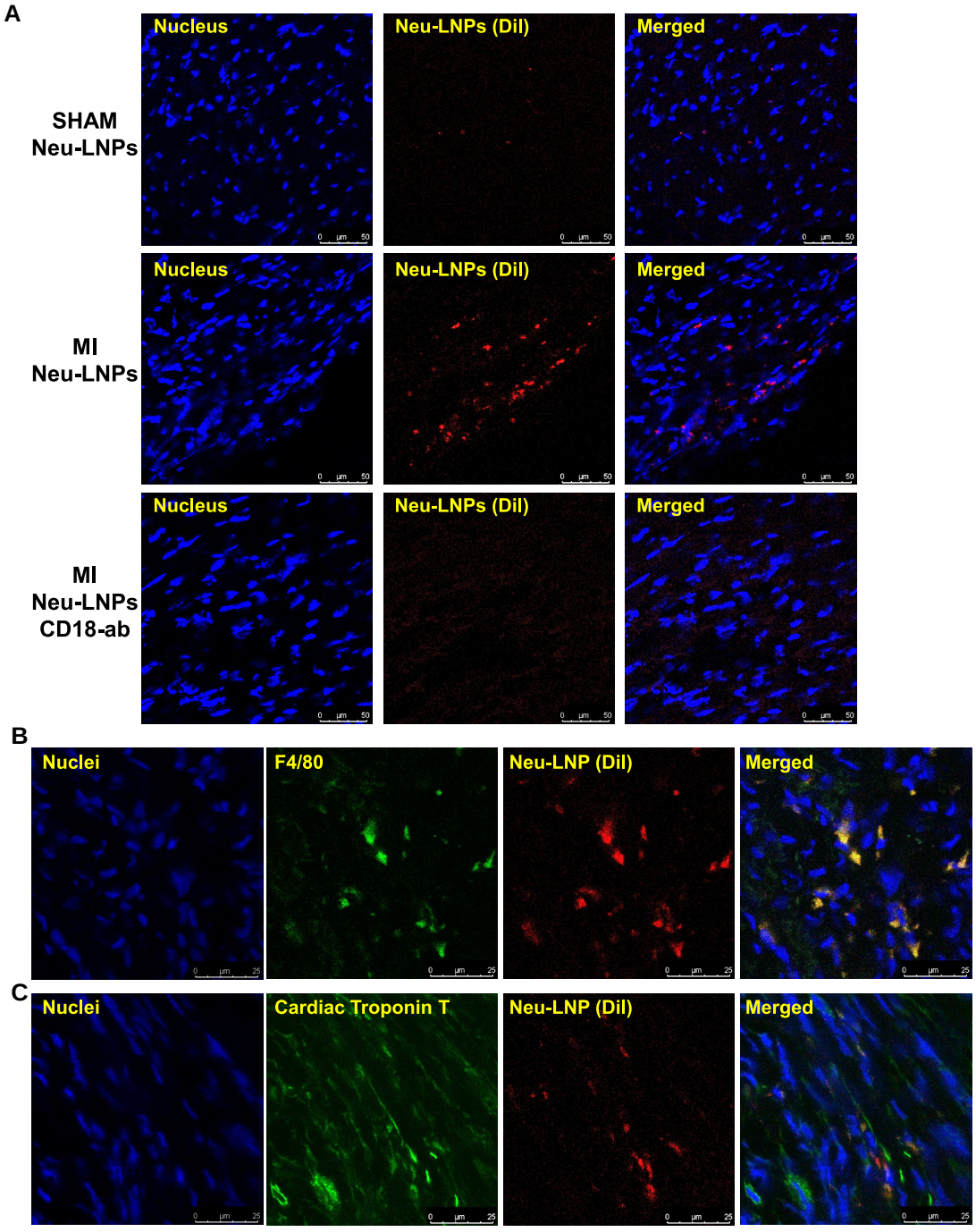

Figure 4 Targeting and cellular uptake analysis of Neu-LNPs *in vivo*. (*A*) Confocal images showing the distribution of Dil-labelled Neu-LNPs in the LV myocardium of SHAM and MI rats administered with Neu-LNPs or MI rats administered with Neu-LNPs incubated with anti-CD18 antibody. Scale bars: 50 μm. $n = 3$ in each group. (*B*, *C*) Confocal immunostaining images displaying the colocalization of Dil-labelled Neu-LNPs with macrophages (*B*) and cardiomyocytes (*C*) in the peri-infarct regions of MI rat hearts. Nuclei were stained with DAPI. Scale bars: 25 μm.

and *E*). Notably, these observations were accompanied with up-regulated mRNA expression of pro-fibrotic markers, collagen-I (*Figure 7F*), collagen-III (*Figure 7G*), and fibronectin (*Figure 7H*) 4 weeks after MI. Treatments with TAPI-1-Neu-LNPs or TAPI-1-LNPs but not TAP1, Neu-LNPs significantly attenuated the mRNA expression of fibronectin, collagen-I, and collagen-III in MI rats, with TAPI-1-Neu-LNPs being most effective in reducing the levels of these pro-fibrotic markers.

3.10 Effect of TAPI-1-Neu-LNPs on immune cell compositions in the heart

To assess the immunomodulation capacity of TAPI-1-Neu-LNPs, we conducted a flow cytometric analysis of immune cell compositions 4 weeks after MI, including CD4+ and CD8+ T cells, NK cells, neutrophils, and two subtypes of monocyte-macrophages (classic $CD43^{low}/HIS48^{high}$ and non-classic $CD43^{high}/HIS48^{low}$) in peri-infarcted area of LV according to

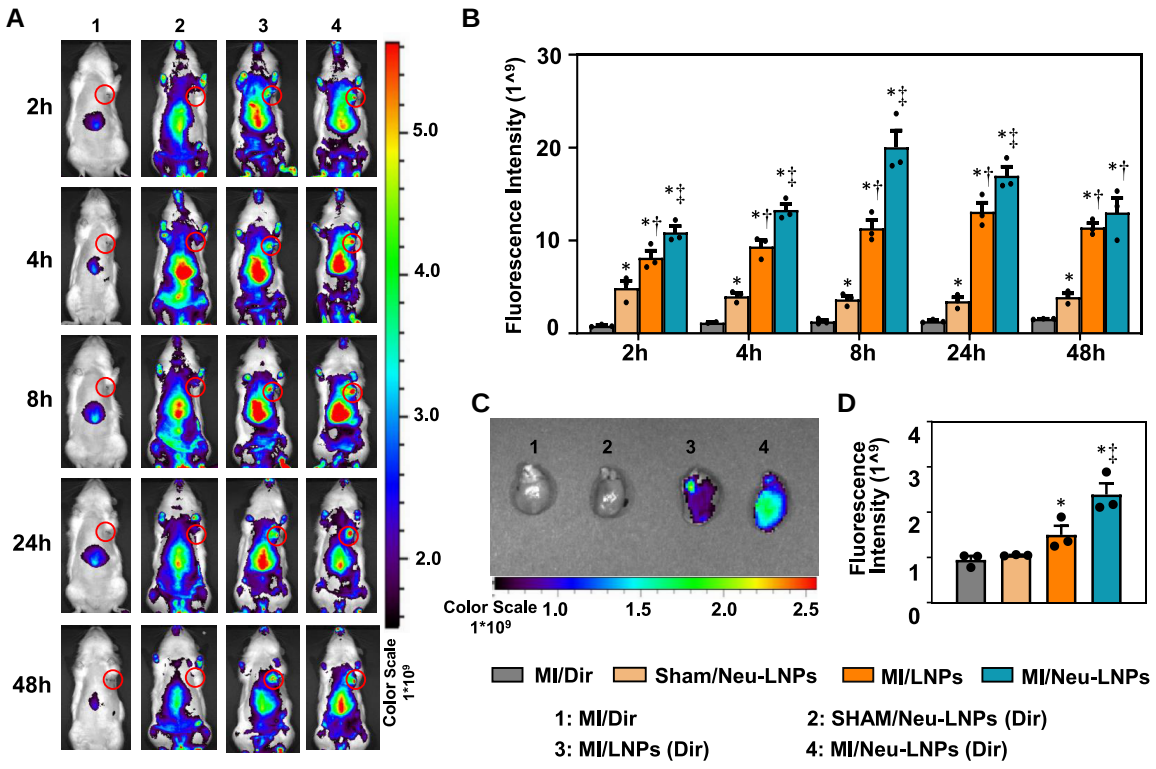

Figure 5 *In vivo* biodistribution analysis of Neu-LNPs. (*A*) *In vivo* small animal imaging exhibits the biodistribution of Dir-labelled LNPs/Neu-LNPs in MI or SHAM rats at different time points within 48 h post-injection. (*B*) Grouped data illustrating quantified fluorescence intensity of Dir-labelled LNPs/Neu-LNPs in the heart at distinct time intervals within the initial 48 h post-injection. (*C*, *D*) *Ex vivo* fluorescence image and quantification of fluorescence intensity of the heart at 48 h after LNPs/Neu-LNPs injection. $n = 3$ in each group, $^{*}P < 0.05$ vs. MI/Dir, $^{\dagger}P < 0.05$ vs. SHAM/Neu-LNPs, $^{\ddagger}P < 0.05$ vs. MI/LNPs. Data set was analysed with two-way ANOVA followed by Sidak's multiple comparisons for *B* and with one-way ANOVA followed by Tukey's multiple comparisons for *D*.

the gating strategy for assessment of major leucocyte subsets (see Supplementary material online, *Figure S9*). Our findings revealed that CD4+ (see Supplementary material online, *Figure S10A*), CD8+ T cells (see Supplementary material online, *Figure S10B*), NK cells (see Supplementary material online, *Figure S10C*), neutrophils (see Supplementary material online, *Figure S10D*), and $CD43^{low}/HIS48^{high}$ monocyte-macrophages (see Supplementary material online, *Figure S10E*) were higher in MI compared to SHAM rats, while there was no significant change in $CD43^{high}/HIS48^{low}$ monocyte-macrophages (see Supplementary material online, *Figure S10F*). Despite a trend of reduction in the percentage of these immune cells following a 4-week treatment with TAPI-1-LNPs or TAPI-1 alone, statistical significance was not attained in some cases compared to MI rats treated with the VEH. However, a 4-week treatment with TAPI-1-Neu-LNPs significantly reduced these immune cell populations when compared to MI rats treated with VEH, and in most cases, the percentage of these cells in MI rats treated with TAPI-1-Neu-LNPs was significantly lower than that in MI groups treated with TAPI-1-LNPs, Neu-LNPs, or TAPI-1. In the case of monocytes, treatment with TAPI-1 alone did not affect both subtypes of monocyte-macrophages in MI rats. On the other hand, HF rats treated with TAPI-1-LNPs had significantly reduced classic $CD43^{low}/HIS48^{high}$ M1 macrophages, but not the non-classic $CD43^{high}/HIS48^{low}$ M2 macrophages. However, treatment with TAPI-1-Neu-LNPs significantly reduced both subtypes of monocytes in MI rats when compared to MI rats treated with the vehicle, TAPI-1, or Neu-LNPs.

4. Discussion

TNF-α is well-documented for its significant role in contributing to cardiac remodelling, fibrosis, and dysfunction in the development of HF.[29,30] However, clinical trials using TNF-α inhibitors like etanercept and infliximab for HF have shown no clinical benefits.[31–33] TNF-α is initially produced as a membrane-bound protein and is activated into its soluble form by proteolytic cleavage by TACE/ADAM17.[34,35] While soluble TNF-α promotes inflammation, transmembrane TNF-α may have anti-inflammatory effects.[36,37] Inhibiting TACE activity, such as with TAPI-1, could reduce soluble TNF-α levels while preserving the potentially beneficial effects of transmembrane TNF-α, offering additional therapeutic potential for HF treatment. In this study, we developed a neutrophil-mimic liposomal nanoparticle for the targeted delivery of a TACE inhibitor TAPI-1 specifically to the infarcted heart and further evaluated its therapeutic effectiveness in rats with MI. Our data revealed that MI rats treated with TAPI-1-Neu-LNPs displayed significant improvements on cardiac dynamics, cardiac fibrosis, and immune cell compositions of the infarcted heart, compared to the treatments with TAPI-1-LNPs, Neu-LNPs, or TAPI-1. Moreover, the Neu-LNPs exhibited minimal cytotoxicity, optimal biocompatibility, and remarkable targeting capability towards the inflamed heart. These outcomes highlight the potential of Neu-LNPs as a potent and efficient tool for drug delivery to enhance therapeutic efficacy in managing cardiac dysfunction and remodelling, thereby address the interventional effectiveness in the treatment of HF.

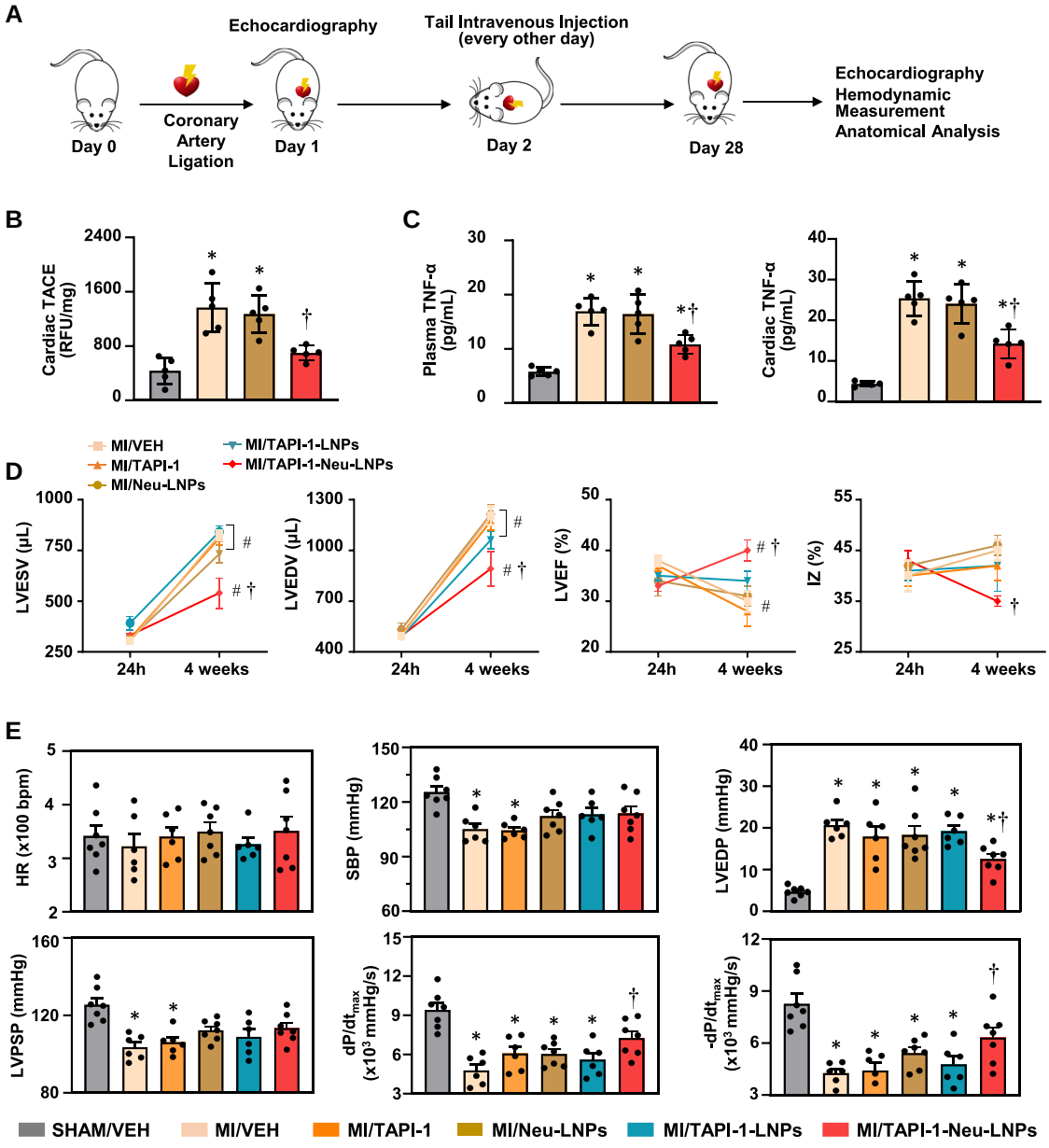

Figure 6 Effect of TAPI-1-Neu-LNPs on the LV function and cardiac dynamics. (*A*) Schematic outlining the experimental design and measurement protocols. (*B*) TACE activity in LV myocardium in SHAM rats treated with vehicle (VEH) and MI rats treated with VEH, Neu-LNPs, or TAPI-1-Neu-LNPs. (*C*) TNF-α levels in plasma and LV myocardium in SHAM rats treated with vehicle (VEH) and MI rats treated with VEH, Neu-LNPs, or TAPI-1-Neu-LNPs. (*D*) Echocardiographic evaluation of LVESV, LVEDV, LVEF, and IZ. (*E*) Analysis of cardiac haemodynamics on HR, SBP, LVEDP, LVPSP, and maximum rates of pressure change during isovolumetric contraction ($+dP/dt_{max}$) and relaxation ($-dP/dt_{max}$) across six experimental groups. LVESV, left ventricular end-systolic volume; LVEDV, LV end-diastolic volume; LVEF, left ventricular ejection fraction; IZ, ischaemic zone; HR, heart rate; SBP, systolic blood pressure; LVEDP, left ventricular end-diastolic pressure; LVPSP, left ventricular peak systolic pressure. $n = 5–7$; $^{\#}P < 0.05$, 4 weeks vs. 24 h; $^{*}P < 0.05$ vs. SHAM/VEH; $^{\dagger}P < 0.05$, MI/TAPI-1-Neu-LNPs vs. MI/VEH, MI/Neu-LNPs, and/or MI/TAPI-1. Data set was analysed with one-way ANOVA followed by Tukey's multiple comparisons for *B*, *C*, and *E* and with two-way ANOVA followed by Sidak's multiple comparisons for *D*.

Neutrophils are among the initial responders to the sites of infection or tissue injury, and play a pivotal role in triggering inflammatory processes.[38] Researchers have leveraged the chemotactic nature of neutrophils to enhance drug delivery capabilities and achieve more precise targeting.[39,40] Drawn by migratory signals, neutrophils rapidly accumulate at injured sites, where they release active mediators, engage in antibody phagocytosis, and eliminate complement-fixed pathogens.[41] Harnessing the ability of neutrophils to navigate inflammation and traverse physiological barriers for tissue penetration, we constructed a nanoparticle platform incorporated with neutrophil membrane proteins for interventional agent delivery. In this Neu-LNPs framework,

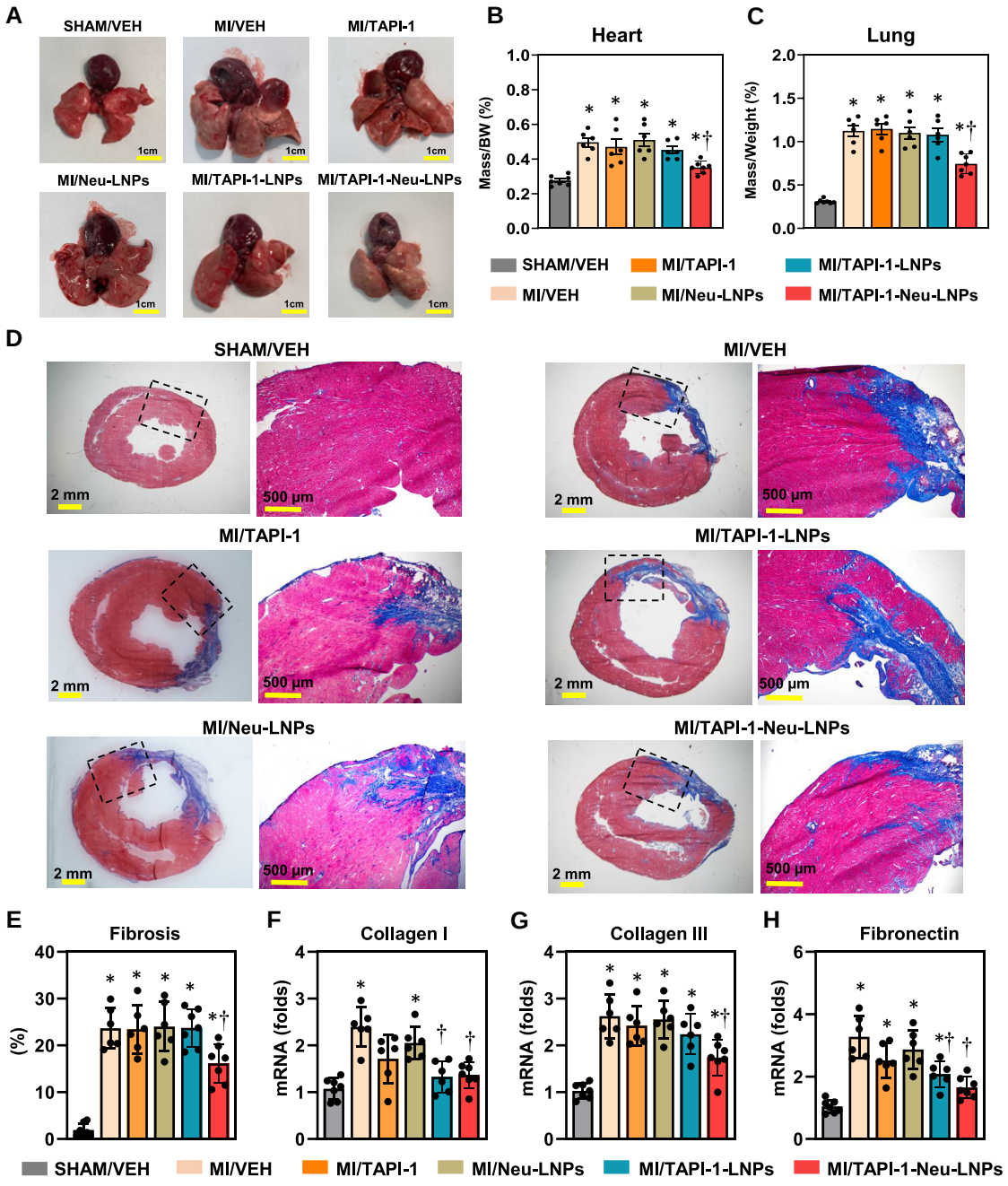

Figure 7 Effect of the TAPI-1-Neu-LNPs on cardiac remodelling. (*A*) Representative images of heart and lung specimens from six experimental groups following a 4-week treatment. (*B*, *C*) Anatomic assessments of heart weight-to-body weight ratio and lung weight-to-body weight ratio. (*D*) Representative Masson's trichrome staining images showing cardiac fibrosis from SHAM or HF rats treated with vehicle (VEH), Neu-LNPs, TAPI-1-LNPs/Neu-LNPs, or TAPI-1 alone. (*E*) Grouped data showing the quantified collagen deposition (%) of the heart. (*F–H*) Comparative quantification of mRNA expression of profibrotic markers collagen-I (*F*), collagen-III (*G*), and fibronectin (*H*) in the peri-infarct regions of the left ventricle across six treatment cohorts. Values are mean ± S.E.M. ($n = 6–7$ for each group). *$P < 0.05$ vs. SHAM/VEH; †$P < 0.05$ vs. MI/VEH. Data set was analysed with one-way ANOVA followed by Tukey's multiple comparisons for *B*, *C*, and *E–H*.

neutrophil membrane fragments derived from LPS-stimulated neutrophils were fused with synthetically crafted liposomal nanoparticles. The inherent stability of the nanoparticle cores, combined with the asymmetrical charge distribution of biological membranes, engenders a core–shell architecture featuring energetically favourable membrane orientation.[9] This core–shell nanostructure retains the primary membrane proteins from neutrophils while maintaining nanoparticle characteristics like size, morphology, and zeta potential. Importantly, the incorporation of neutrophil membrane fragments onto liposomal surfaces had no significant adverse impact on biocompatibility. Furthermore, the bioengineered Neu-LNPs inherit the chemotactic capability associated with inflammation, bolstering their potential as efficient drug delivery tools in clinical contexts for treating HF.

The underlying mechanisms driving the active targeting process and permeability of biomimetic nanoparticles through endothelial layers to reach cardiomyocytes were investigated. Both LFA-1 and Mac-1 are the receptors primarily found on the surface of neutrophils, exhibiting a high affinity for ICAM-1 present on the endothelial cells of inflamed sites.[42,43] In the context of MI, expression of ICAM-1 was up-regulated in endothelial cells of blood vessels in the myocardium of the injured heart.[44] ICAM-1 functions as a cell adhesion molecule that aids in the migration of Neu-LNPs from bloodstream to the inflamed tissues. Once bound to the endothelial cells, the Neu-LNPs are internalized by macrophages through receptor-mediated endocytosis or phagocytosis.[45] This intricate process enables the modified nanoparticles to overcome the endothelial barrier and access the inflamed tissues. Blocking LFA-1/Mac-1 on Neu-LNPs resulted in a decrease in cellular uptake *in vitro* and the absence of Neu-LNPs in myocardium of infarcted heart *in vivo*, highlighting the interplay of LFA1/Mac1/ICAM-1 in directing Neu-LNPs to inflammation sites. Taken together, our data indicated that the coordinated interaction between LFA-1/Mac-1 with overexpressed ICAM-1 in peri-infarct zone of the hearts with MI, driven by integrin-mediated adhesion mechanisms, enhances the targeting ability and the permeation capability of Neu-LNPs across endothelial layers, facilitating their access to inflamed cardiomyocytes.

Liposome synthesis represents a robust nanotechnology that has demonstrated both efficacy and safety, establishing itself as a widely utilized formulation of nanoparticles over the past several decades.[46] The Neu-LNPs platform capitalizes on the advantageous pharmacokinetic characteristics of liposomes, coupled with the simplicity of membrane fusion for targeted modification of nanoparticles towards to inflammatory sites. POPE-PEG_{2000} is a key constituent in the synthesis of Neu-LNPs. PEGylation, a commonly employed technique, involves covalently binding PEG chains to the nanoparticle surface, thereby introducing a steric hindrance that prevents close interactions between particles to enhance the stability and accumulation of nanoparticles.[14] Additionally, PEGylation serves to curtail protein opsonization—an immune system-mediated clearance process—by creating a hydrophilic PEG layer on the nanoparticle surface. Furthermore, PEGylation extends the circulation half-life of nanoparticles by diminishing their recognition and uptake by the reticuloendothelial system. The PEG corona shields the nanoparticles from engulfment and clearance by phagocytic cells, facilitating prolonged circulation in the bloodstream. This extended circulation half-life significantly enhances the nanoparticle's ability to amass at inflamed sites, such as the infarcted zone after MI. The protracted blood half-life of PEGylated nanoparticles improves their extravasation and accumulation at the inflamed sites, especially when capitalizing on the EPR effect exploited by PEGylated nanoparticles.

The cardiac targeting potential and blood circulation longevity of the biomimetic nanoparticles were assessed using non-invasive *in vivo* small animal imaging. While Dir-labelled Neu-LNPs injected via tail veins exhibited significant accumulation in the infarcted heart in MI rats, they were scarcely detected in the heart of SHAM rats. Additionally, in MI rats injected with Dir alone, the dye signals were predominantly visualized in the liver rather than the heart. These findings imply that the specifically designed Neu-LNPs would target primarily the inflammatory sites despite their distribution throughout the body post-injection. Additionally, both Neu-LNPs and LNPs were obviously detected within 24 h following injection in either SHAM or MI rats, and remained elevated at 48 h and beyond. However, MI rats receiving only Dir exhibited minimal dye signal visibility at 48 h, with detection primarily limited to the initial 24 h timeframe. These observations highlight the capacity of Neu-LNPs to enhance targeted delivery to the inflamed heart in MI conditions, concurrently with an extended circulation duration.

Notably, both MI and SHAM rats exhibited substantial accumulation of Neu-LNPs in the liver, with significantly higher levels in MI rats. The heightened inflammatory response in MI increases immune cell infiltration in the heart and raises immune cell levels in the blood. The liver, being a key metabolic and innate defense organ, rich in macrophages and Kupffer cells, actively clears excess immune cells and foreign entities such as nanoparticles. The specially designed Neu-LNPs display a targeted affinity for immune cells that are more abundant in the liver in the condition of MI, making Neu-LNPs more likely to be captured in the liver of MI rats. Also, congestive hepatopathy, a condition associated with MI, causes blood to back up in the liver, further enhancing nanoparticle retention. Despite predominantly accumulating in the liver, Neu-LNPs did not significantly affect serum levels of alanine aminotransferase or aspartate aminotransferase (see Supplementary material online, *Table S4*), nor did they alter the liver tissue architecture as observed in H&E staining (see Supplementary material online, *Figure S11A*), indicating an absence of liver dysfunction or hepatotoxicity. Furthermore, tail vein injection of Neu-LNPs did not result in significant changes in haematological parameters, biochemical markers of renal function (see Supplementary material online, *Table S4*), or glomerular and tubular structures observed in kidney H&E staining in rats (see Supplementary material online, *Figure S11B*).

The ectodomain shedding of active soluble TNF-α by TACE is of paramount importance for TNF-α-driven inflammation in HF and various inflammatory ailments. The expression of TACE was remarkably elevated in the HF patients, with levels increasing in accordance with the severity of cardiac compromise.[47,48] In this work, we discovered that systemic administration of TACE inhibitor TAPI-1 encapsulated within the Neu-LNPs in MI rats led to an improvement in post-infarct LV dysfunction, pulmonary congestion, cardiac contractility, and remodelling processes in the peri-infarcted region, surpassing those observations in other treatment groups with TAPI-1-LNPs or TAPI-1 alone. MI rats treated solely with Neu-LNPs did not demonstrate beneficial effects on cardiac function and remodelling, suggesting that suppressing TACE using TAPI-1 delivered via Neu-LNPs holds therapeutic potential for ameliorating the cardiac manifestations in the clinical setting of HF. Although other treatment groups with TAPI-1 also exhibited certain degrees of protective effects in MI rats, TAPI-1-Neu-LNPs displayed superior efficiency compared to TAPI-1 or TAPI-1 delivered via non-modified LNPs.

Furthermore, MI rats treated with TAPI-1-Neu-LNPs displayed a significant reduction in inflammatory responses, accompanied with a diminished immune cell presence within the peri-infarct zone of the heart. The attenuation of actively proliferating immune cells within the surrounding area of infarcted zone of MI heart is most likely a potential mechanism for the role of TAPI-1 in cardiac dynamics and cardiac remodelling. Notably, the injected Neu-LNPs were internalized by both macrophages and cardiomyocytes, both of which contribute to the production of TNF-α in ischaemic myocardium.[26,27,49] It should be mentioned that while TAPI-1, as a TACE inhibitor, prevents the production of TNF-α from both cell types, it also inhibits other metallopeptidases such as ADAM10 produced by cardiomyocytes, potentially offering a beneficial effect on cardiac function through this additional mechanism.

4.1 Study limitations

Several limitations need to be addressed for this study. First, although Neu-LNP also accumulated in the liver and spleen, the study did not examine whether TAPI-1-Neu-LNPs can reduce inflammation in these organs to improve cardiac function and remodelling. Due to the notable absence of Neu-LNP accumulation in the lungs, the reduced pulmonary congestion in MI rats treated with TAPI-1-Neu-LNPs is likely a result of its action in reducing the preload of the heart, rather than directly reducing inflammation in this organ. Secondly, the assessments of pro-fibrosis markers or immune cell compositions were conducted 4 weeks after MI. It should be aware that changes in mRNA levels of these markers or immune cell infiltration likely occurred during the early stages of MI and may be more pronounced than those observed 4 weeks post-MI at the established stages. Additionally, post-MI cardiac remodelling or inflammatory response is a dynamic process, especially in the border regions of the MI. This process can continue progressively for 4–6 weeks until eventual scar formation in the infarcted heart.[50,51] Thus, discontinuing treatment with TAPI-1-Neu-LNPs at this stage could significantly deteriorate cardiac remodelling and pulmonary oedema. However, the long-term effects of stopping TAPI-1-Neu-LNPs treatment remain uncertain, and we are interested in exploring this question in future studies. Lastly, this study exclusively

involved male rats for a more targeted investigation into sex-specific effects of interventions or treatments, without the potential confounding influence of hormonal fluctuation. Further research with female subjects is warranted to assess potential sex differences in enhancing therapeutic efficiency using TAPI-1-Neu-LNPs for treating HF.

4.2 Conclusions

Biomimetic drug carriers, particularly those cell membrane-coated nanoparticles, are a promising therapeutic framework for addressing the delivery effectiveness and the safety. The demonstrated outcomes in MI rats treated with TAPI-1-Neu-LNPs provide compelling evidence for the use of Neu-LNPs to offer an additional layer of protection, acting as a conduit for enhancing the precise delivery of therapeutic agents to the targets. The insights gleaned from this investigation lay the groundwork for the prospective clinical application of Neu-LNPs as an innovative approach to amplify the therapeutic impact of interventions in HF, with potential extensions to various pathological conditions characterized by elevated inflammatory states.

Translational perspective

A nanoparticle platform engineered with neutrophil membrane fragments demonstrated significant targeting capability to the infarcted heart in rats with myocardial infarction. Pharmacological interventions aiming to suppress TACE/ADAM17 activity within the inflamed heart, facilitated by biomimetic nanoparticles, can provide an additional layer of protection to enhance left ventricular function and alleviate cardiac remodelling in the context of heart failure induced by myocardial infarction. The demonstrated efficacy of neutrophil-mimic liposomal nanoparticles in this work warrants careful consideration for their translation into clinical practice and highlights the potential of nanoparticles as an effective drug delivery strategy in the treatments of cardiovascular disorders.

Supplementary material

Supplementary material is available at *Cardiovascular Research* online.

Acknowledgements

We acknowledge Kathy Zimmerman, RDCS, for diligent and expert assistance in the performance of the echocardiograms to assess cardiac function.

Conflict of interest: none declared.

Funding

This work was supported by research grants from National Heart, Lung, and Blood Institute of the National Institutes of Health under award numbers R01 HL-139521 and HL-155091 (to S.-G.W.), and 1S10-OD019941 (to R.M.W.). The content is solely the responsibility of the authors and does not necessarily represent the official views of the National Institutes of Health.

Data availability

The data underlying this article are available in the article and in its online supplementary material.

References

1. Sindhwani S, Chan WCW. Nanotechnology for modern medicine: next step towards clinical translation. *J Intern Med* 2021;**290**:486–498.
2. Bayda S, Adeel M, Tuccinardi T, Cordani M, Rizzolio F. The history of nanoscience and nanotechnology: from chemical–physical applications to nanomedicine. *Molecules* 2019;**25**:112.
3. Mitchell MJ, Billingsley MM, Haley RM, Wechsler ME, Peppas NA, Langer R. Engineering precision nanoparticles for drug delivery. *Nat Rev Drug Discov* 2021;**20**:101–124.
4. Steichen SD, Caldorera-Moore M, Peppas NA. A review of current nanoparticle and targeting moieties for the delivery of cancer therapeutics. *Eur J Pharm Sci* 2013;**48**:416–427.
5. Walkey CD, Olsen JB, Guo H, Emili A, Chan WC. Nanoparticle size and surface chemistry determine serum protein adsorption and macrophage uptake. *J Am Chem Soc* 2012;**134**:2139–2147.
6. Yetisgin AA, Cetinel S, Zuvin M, Kosar A, Kutlu O. Therapeutic nanoparticles and their targeted delivery applications. *Molecules* 2020;**25**:2193.
7. Yaman S, Chintapula U, Rodriguez E, Ramachandramoorthy H, Nguyen KT. Cell-mediated and cell membrane-coated nanoparticles for drug delivery and cancer therapy. *Cancer Drug Resist* 2020;**3**:879–911.
8. Luk BT, Zhang L. Cell membrane-camouflaged nanoparticles for drug delivery. *J Control Release* 2015;**220**:600–607.
9. Fang RH, Kroll AV, Gao W, Zhang L. Cell membrane coating nanotechnology. *Adv Mater* 2018;**30**:e1706759.
10. McLean MA, Gregory MC, Sligar SG. Nanodiscs: a controlled bilayer surface for the study of membrane proteins. *Annu Rev Biophys* 2018;**47**:107–124.
11. Narain A, Asawa S, Chhabria V, Patil-Sen Y. Cell membrane coated nanoparticles: next-generation therapeutics. *Nanomedicine (Lond)* 2017;**12**:2677–2692.
12. Zhu C, Ma J, Ji Z, Shen J, Wang Q. Recent advances of cell membrane coated nanoparticles in treating cardiovascular disorders. *Molecules* 2021;**26**:3428.
13. Stapleton S, Milosevic M, Allen C, Zheng J, Dunne M, Yeung I, Jaffray DA. A mathematical model of the enhanced permeability and retention effect for liposome transport in solid tumors. *PLoS One* 2013;**8**:e81157.
14. Suk JS, Xu Q, Kim N, Hanes J, Ensign LM. PEGylation as a strategy for improving nanoparticle-based drug and gene delivery. *Adv Drug Deliv Rev* 2016;**99**:28–51.
15. Butterfield TA, Best TM, Merrick MA. The dual roles of neutrophils and macrophages in inflammation: a critical balance between tissue damage and repair. *J Athl Train* 2006;**41**:457–465.
16. Black RA, Rauch CT, Kozlosky CJ, Peschon JJ, Slack JL, Wolfson MF, Castner BJ, Stocking KL, Reddy P, Srinivasan S, Nelson N, Boiani N, Schooley KA, Gerhart M, Davis R, Fitzner JN, Johnson RS, Paxton RJ, March CJ, Cerretti DP. A metalloproteinase disintegrin that releases tumour-necrosis factor-alpha from cells. *Nature* 1997;**385**:729–733.
17. Yu Y, Xue B, Irfan NM, Beltz T, Weiss RM, Johnson AK, Felder RB, Wei SG. Reducing brain TACE activity improves neuroinflammation and cardiac function in heart failure rats. *Front Physiol* 2022;**13**:1052304.
18. Yu Y, Cao Y, Bell B, Chen X, Weiss RM, Felder RB, Wei SG. Brain TACE (tumor necrosis factor-alpha-converting enzyme) contributes to sympathetic excitation in heart failure rats. *Hypertension* 2019;**74**:63–72.
19. Yu Y, Weiss RM, Wei SG. Brain interleukin-17A contributes to neuroinflammation and cardiac dysfunction in rats with myocardial infarction. *Front Neurosci* 2022;**16**:1032434.
20. Yu Y, Chen E, Weiss RM, Felder RB, Wei SG. Transforming growth factor-alpha acts in hypothalamic paraventricular nucleus to upregulate ERK1/2 signaling and expression of sympathoexcitatory mediators in heart failure rats. *Neuroscience* 2022;**483**:13–23.
21. Hu CM, Fang RH, Wang KC, Luk BT, Thamphiwatana S, Dehaini D, Nguyen P, Angsantikul P, Wen CH, Kroll AV, Carpenter C, Ramesh M, Qu V, Patel SH, Zhu J, Shi W, Hofman FM, Chen TC, Gao W, Zhang K, Chien S, Zhang L. Nanoparticle biointerfacing by platelet membrane cloaking. *Nature* 2015;**526**:118–121.
22. Zhang H. Thin-film hydration followed by extrusion method for liposome preparation. In: D'Souza GGM (ed.), *Liposomes: Methods and Protocols*. New York, NY: Springer New York; 2017. p17–22.
23. Marchi LF, Sesti-Costa R, Chedraoui-Silva S, Mantovani B. Comparison of four methods for the isolation of murine blood neutrophils with respect to the release of reactive oxygen and nitrogen species and the expression of immunological receptors. *Comp Clin Path* 2014;**23**:1469–1476.
24. Molinaro R, Corbo C, Martinez JO, Taraballi F, Evangelopoulos M, Minardi S, Yazdi IK, Zhao P, De Rosa E, Sherman MB, De Vita A, Toledano Furman NE, Wang X, Parodi A, Tasciotti E. Biomimetic proteolipid vesicles for targeting inflamed tissues. *Nat Mater* 2016;**15**:1037–1046.
25. Mereghetti P, Corsetto PA, Cremona A, Rizzo AM, Doglia SM, Ami D. A Fourier transform infrared spectroscopy study of cell membrane domain modifications induced by docosahexaenoic acid. *Biochimica et Biophysica Acta (BBA)—General Subjects* 2014;**1840**:3115–3122.
26. Irwin MW, Mak S, Mann DL, Qu R, Penninger JM, Yan A, Dawood F, Wen WH, Shou Z, Liu P. Tissue expression and immunolocalization of tumor necrosis factor-alpha in postinfarction dysfunctional myocardium. *Circulation* 1999;**99**:1492–1498.

27. Chen Y, Pat B, Zheng J, Cain L, Powell P, Shi K, Sabri A, Husain A, Dell'italia LJ. Tumor necrosis factor-alpha produced in cardiomyocytes mediates a predominant myocardial inflammatory response to stretch in early volume overload. *J Mol Cell Cardiol* 2010;**49**:70–78.
28. Sultana S, Bishayi B. Potential anti-arthritic and anti-inflammatory effects of TNF-alpha processing inhibitor-1 (TAPI-1): a new approach to the treatment of S. aureus arthritis. *Immunobiology* 2020;**225**:151887.
29. Torre-Amione G, Bozkurt B, Deswal A, Mann DL. An overview of tumor necrosis factor alpha and the failing human heart. *Curr Opin Cardiol* 1999;**14**:206–210.
30. Feldman AM, Combes A, Wagner D, Kadakomi T, Kubota T, Li YY, McTiernan C. The role of tumor necrosis factor in the pathophysiology of heart failure. *J Am Coll Cardiol* 2000;**35**: 537–544.
31. Krum H. Tumor necrosis factor-alpha blockade as a therapeutic strategy in heart failure (RENEWAL and ATTACH): unsuccessful, to be specific. *J Card Fail* 2002;**8**:365–368.
32. Mann DL, McMurray JJ, Packer M, Swedberg K, Borer JS, Colucci WS, Djian J, Drexler H, Feldman A, Kober L, Krum H, Liu P, Nieminen M, Tavazzi L, van Veldhuisen DJ, Waldenstrom A, Warren M, Westheim A, Zannad F, Fleming T. Targeted anticytokine therapy in patients with chronic heart failure: results of the Randomized Etanercept Worldwide Evaluation (RENEWAL). *Circulation* 2004;**109**:1594–1602.
33. Chung ES, Packer M, Lo KH, Fasanmade AA, Willerson JT; Anti-TNF Therapy Against Congestive Heart Failure Investigators. Randomized, double-blind, placebo-controlled, pilot trial of infliximab, a chimeric monoclonal antibody to tumor necrosis factor-alpha, in patients with moderate-to-severe heart failure: results of the anti-TNF Therapy Against Congestive Heart Failure (ATTACH) trial. *Circulation* 2003;**107**:3133–3140.
34. Horiuchi K. A brief history of tumor necrosis factor alpha-converting enzyme: an overview of ectodomain shedding. *Keio J Med* 2013;**62**:29–36.
35. Gearing AJ, Beckett P, Christodoulou M, Churchill M, Clements J, Davidson AH, Drummond AH, Galloway WA, Gilbert R, Gordon JL, Leber TM, Mangan M, Miller K, Nayee P, Owen K, Patel S, Thomas W, Wells G, Wood LM, Woolley K. Processing of tumour necrosis factor-alpha precursor by metalloproteinases. *Nature* 1994;**370**:555–557.
36. Schulz R, Heusch G. Tumor necrosis factor-alpha and its receptors 1 and 2: yin and yang in myocardial infarction? *Circulation* 2009;**119**:1355–1357.
37. Monden Y, Kubota T, Inoue T, Tsutsumi T, Kawano S, Ide T, Tsutsui H, Sunagawa K. Tumor necrosis factor-alpha is toxic via receptor 1 and protective via receptor 2 in a murine model of myocardial infarction. *Am J Physiol Heart Circ Physiol* 2007;**293**:H743–H753.
38. Herrero-Cervera A, Soehnlein O, Kenne E. Neutrophils in chronic inflammatory diseases. *Cell Mol Immunol* 2022;**19**:177–191.
39. Metzemaekers M, Gouwy M, Proost P. Neutrophil chemoattractant receptors in health and disease: double-edged swords. *Cell Mol Immunol* 2020;**17**:433–450.
40. Wang H, Zang J, Zhao Z, Zhang Q, Chen S. The advances of neutrophil-derived effective drug delivery systems: a key review of managing tumors and inflammation. *Int J Nanomedicine* 2021;**16**:7663–7681.
41. de Oliveira S, Rosowski EE, Huttenlocher A. Neutrophil migration in infection and wound repair: going forward in reverse. *Nat Rev Immunol* 2016;**16**:378–391.
42. Li N, Yang H, Wang M, Lu S, Zhang Y, Long M. Ligand-specific binding forces of LFA-1 and Mac-1 in neutrophil adhesion and crawling. *Mol Biol Cell* 2018;**29**:408–418.
43. Mazzone A, Ricevuti G. Leukocyte CD11/CD18 integrins: biological and clinical relevance. *Haematologica* 1995;**80**:161–175.
44. Niessen HW, Lagrand WK, Visser CA, Meijer CJ, Hack CE. Upregulation of ICAM-1 on cardiomyocytes in jeopardized human myocardium during infarction. *Cardiovasc Res* 1999;**41**: 603–610.
45. Sousa de Almeida M, Susnik E, Drasler B, Taladriz-Blanco P, Petri-Fink A, Rothen-Rutishauser B. Understanding nanoparticle endocytosis to improve targeting strategies in nanomedicine. *Chem Soc Rev* 2021;**50**:5397–5434.
46. Lujan H, Griffin WC, Taube JH, Sayes CM. Synthesis and characterization of nanometer-sized liposomes for encapsulation and microRNA transfer to breast cancer cells. *Int J Nanomedicine* 2019;**14**:5159–5173.
47. Shimoda Y, Satoh M, Nakamura M, Akatsu T, Hiramori K. Activated tumour necrosis factor-alpha shedding process is associated with in-hospital complication in patients with acute myocardial infarction. *Clin Sci (Lond)* 2005;**108**:339–347.
48. Akatsu T, Nakamura M, Satoh M, Hiramori K. Increased mRNA expression of tumour necrosis factor-alpha and its converting enzyme in circulating leucocytes of patients with acute myocardial infarction. *Clin Sci (Lond)* 2003;**105**:39–44.
49. Torre-Amione G, Kapadia S, Lee J, Durand JB, Bies RD, Young JB, Mann DL. Tumor necrosis factor-alpha and tumor necrosis factor receptors in the failing human heart. *Circulation* 1996; **93**:704–711.
50. Ghafoor M, Kamal M, Nadeem U, Husain AN. Educational case: myocardial infarction: histopathology and timing of changes. *Acad Pathol* 2020;**7**:2374289520976639.
51. Inoue K, Kusachi S, Niiya K, Kajikawa Y, Tsuji T. Sequential changes in the distribution of type I and III collagens in the infarct zone: immunohistochemical study of experimental myocardial infarction in the rat. *Coron Artery Dis* 1995;**6**:153–158.